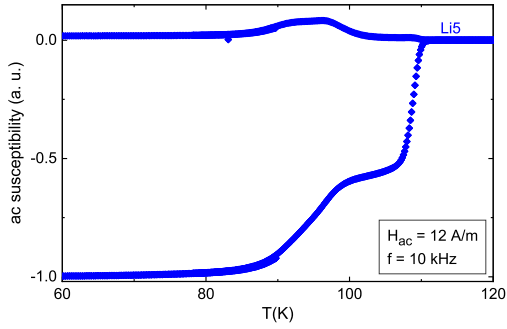
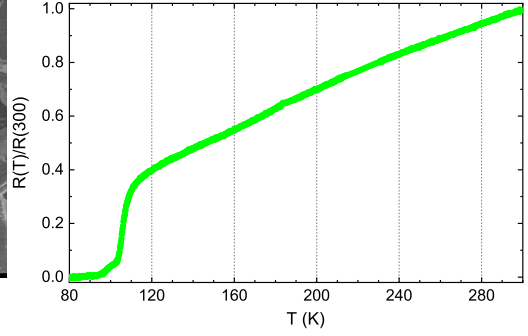
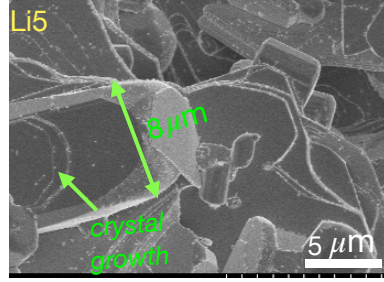


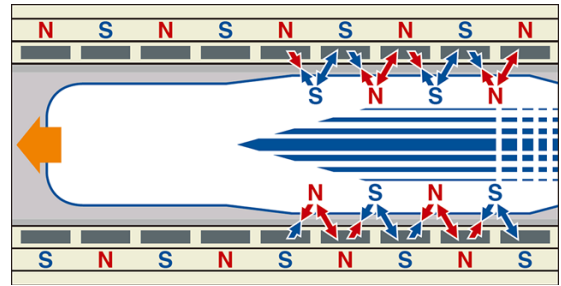
Graphical Abstract

Fingerprint of T_c advancement in Li-doped Bi-2223 superconductors prepared by cationic molecular mixing within Pechini sol-gel synthesis

N. K. Man, Huu T. Do, Nguyen V. Tu, Nguyen V. Quy



SC sample



Superconducting magnet in SCMaglev train (japan.go.jp)

Fingerprint of T_c advancement in Li-doped Bi-2223 superconductors prepared by cationic molecular mixing within Pechini sol-gel synthesis

N. K. Man^a, Huu T. Do^{b,c,*}, Nguyen V. Tu^a, Nguyen V. Quy^a

^a*School of Materials Science and Engineering, Hanoi University of Science and Technology, Hanoi 100000, Vietnam*

^b*Institute of Theoretical and Applied Research, Duy Tan University, Hanoi, 100000, Vietnam*

^c*Faculty of Natural Sciences, Duy Tan University, Da Nang, 550000, Vietnam*

Abstract

Trilayered Bi-2223 superconductor features the highest critical temperature T_c among the bismuth-based cuprate collection and symbolizes an ideal prototype for studying intrinsic superconducting properties. The previous solid-state reaction method substantiated the growth of the high-quality Bi-2223 compounds but was accompanied by excessively laborious time and effort in terms of multiple grinding, pressing, as well as calcining stages, so finding a less tedious synthesis path is imperative. Here, we present an advanced sol-gel synthesis for assembling the multicomponent complexity of $\text{Bi}_{1.4}\text{Pb}_{0.6}\text{Sr}_2\text{Ca}_2(\text{Cu}_{1-x}\text{Li}_x)_3\text{O}_{10+\delta}$ superconductors (Li-doped Bi-2223), with $x = 0.0\text{--}0.20$, utilizing metallic cationic molecular mixing within the chemical Pechini polyesterization route followed by single-step pyrolysis and sintering stages. Although monovalent cations such as Li^+ pose limitations in establishing a perplex crosslinking network or chelating mechanism in the Pechini method, they represent a unique probe to elucidate the major chemical process during polymerization. We observe that a 5 molar % Li-doped sample pronounces the highest $T_c = 111.4$ K among the series of samples, as confirmed by both ac susceptibility and dc resistivity measurements, and is equivalent to the value obtained by our preceding solid state fabrication. In addition, we showcase a rare observation of layer-by-layer crystalline phase growth under microstructure probe. Through analyzing the reliable ac susceptibility data at low magnetic fields in a wide range of frequency, we provide the quantum flux formation and flux creep mechanism by Anderson-Müller's model and Cole-Cole plot. Our study paves a perspicuous pathway for finding effective fabrication for the high-quality Bi-2223 compounds as well as impurity-doped counterparts, by utilizing the appropriate synthesizing and doping processes.

Keywords: Pechini sol-gel route, Li-doping effect, triple-layered Bi-2223 superconductor, CuO_2 plane, crystal growth, critical temperature.

1. Introduction

The dawn of high- T_c superconductivity ignited in partial Ba-replaced La-Cu-O ceramic compounds containing mainstream copper-oxide ingredients, CuO_2 layers, which were categorized as cuprate materials and pronounced the first observation of the transition temperature $T_c = 35$ K [1] above conventional Nb-based metallic alloys [2–5]. Following the class of rare earth RE-Ba-Cu-O materials emerges as $T_c = 90$ K [6], featuring the first superconducting material that works above the abundant liquid nitrogen of 77 K, but accompanied by a typically weak chemical and structural stability due to oxygen loss, losing superconductivity, moisture corrosion, and expensive RE-containing [7, 8]. The most stable group of cuprate compounds without having RE or toxic components refers to the bismuth-based family generalized by the chemical formula $\text{Bi}_2\text{Sr}_2\text{Ca}_{n-1}\text{Cu}_n\text{O}_{2n+4}$ (BSCCO) symbolizes an ideal platform for chemical and structural stability escorted with T_c pursuing a bell-curve shape with respect to the number of cuprate layers, such as 36 K for single-layered Bi-2201 ($n = 1$), elevating to double-layer of 92 K for Bi-2212 ($n = 2$), reaching 110 K for Bi-2223 ($n = 3$), but drastically downturn to 90 K for Bi-2234 ($n = 4$) [9–12]. However, the

*Corresponding author

Email address: huutdo09@gmail.com (Huu T. Do)

BSCCO family, especially for the triple-layered Bi-2223 materials, faces a multitude of difficulties in fabricating high-quality samples in single-phase or homogeneous single crystal forms while they often consist of unwanted impurities pervading in the grain boundary [13, 14]. Therefore, considerable experimental efforts have been employed to elucidate perspicuous pathways to synthesize high-quality Bi-2223 compounds as well as to raise their critical temperatures higher, typically renovating a conventional solid-state [15–17], performing atomic mixing coprecipitation [18, 19], spay-pyrolysis [20, 21], wire or tapes [22, 23], growing single crystal form [24, 25], chemical sol-gel [26–28] and subsequently fabricating thin film [14, 29]. Due to the intrinsic complexity of the multicomponent BSCCO category, the conventional solid-state reaction still retains the most widespread auspicious way to grow a high-quality bulk sample in a mass quantities for traditional known applications such as superconducting bulk magnets or wires [30], but it is intractable to fabricate fine single crystal, thin film, and other superconducting devices for various appliances, such as high- T_c superconducting terahertz devices and quantum interference instruments [25, 27, 31–33].

Among various atomic mixing techniques, sol-gel engages a promising approach; however, a traditional sol-gel synthesis relying on metallic alkoxide precursors has not been proven to be relevant and useful for preparing a complicated multicomponent BSCCO sample caused by a substantial hydrolysis rate difference of Bi, Pb, Sr, Ca and Cu alkoxides as well as the poor solubility of Cu-alkoxide [26, 34]. A state-of-the-art sol-gel technique based on a polymerization or polyesterization process, renowned Pechini method, aims to provide better quality through a selection of chelating agents such as citric acid, acetic acid, ethylenediaminetetraacetic acid, etc. which entrap metallic ions in a complex solution up to homogeneous gel formation [26, 34, 35] or starting from different precursors either nitrate, acetate salts, and carbonate [27]. As in our search of several attempts on the Pechini route, only a few of them provided high-quality samples that exhibited a sharp superconducting transition around 110 K such as growing single crystals from sol-gel precursor [25], adding TiO_2 nanoparticles into Bi-2223 ceramics [28], utilizing different salt precursors [27] or the recent fabrication of thin film from sol-gel synthesis [14]; however, detailed chemical formations have not been intensively advocated. In addition, $T_c = 110.5\text{--}111$ K typifies the highest value recorded for pristine Bi-2223 material by magnetic susceptibility measurements [15, 24, 25, 36], but the samples synthesized by the latest sol-gel technology have not surpassed to the optimum [14, 26, 37].

Inspiring the genesis of high- T_c superconductivity in cuprate compounds results in appending charge carriers either electrons or holes into Mott insulators, e.g., partially replacing external Ba^{2+} for La^{3+} cations [1] or tuning internal oxygen content within the prototypical La_2CuO_4 insulators [38, 39]. In accordance with the indispensable correlation between the fabrication–structure–property principle, varying elemental components does not only modify fabricating technology of Bi-2223 materials, but also alters the superconducting properties. For instance, partial replacement of Pb for Bi reduces the sintering time and temperature as well as creating a favorable liquid phase Ca_2PbO_4 that promotes high- T_c Bi-2223 crystalline growth [15, 40–42]. Intercalating silver oxide into the Bi-2223 frame decreases the sintering time as a catalytic agent, but improves high- T_c grain connectivity [43–45]. Furthermore, partially replacing transition metal oxides of Ni^{2+} , $\text{Fe}^{2+}/\text{Fe}^{3+}$, and Co^{2+} for Cu^{2+} cation in Bi-2223 compounds reduces T_c but an appropriate content enhances pinning force and possible critical current density [46–52]. It has been suggested that presenting TiO_2 nanoparticles between grains improves the connectivity and alignments in the synthesized compounds but reduces the critical temperature [28]. Doping Li_2O into Bi-2223 cuprate reduced the sintering temperature and showcased the sign of T_c elevation observed in previous experiments [15, 53, 54]. However, performance of Li-doped cases by atomic mixing sol-gel synthesis has not been processed. To the best of our knowledge, a comprehensive and thorough interpretation of the chemistry involved in the complex organic polymeric Pechini pathway to synthesize Bi-2223 sample is not apparently stated.

In short, we report our detailed study of chemical evolution with direct substitution of Li^+ for Cu^{2+} cations within the notable Pechini sol-gel route. After that, we demonstrate the characterizing technique to investigate the crystal structure, morphological topography, as well as focused critical temperature and intrinsic superconducting properties in Li-doped Bi(Pb)-2223 frameworks. In further elucidating the flux creep properties, we utilized the Anderson–Müller’s analysis and Cole–Cole plot applying to a wide range of frequencies to elucidate the flux creep formation.

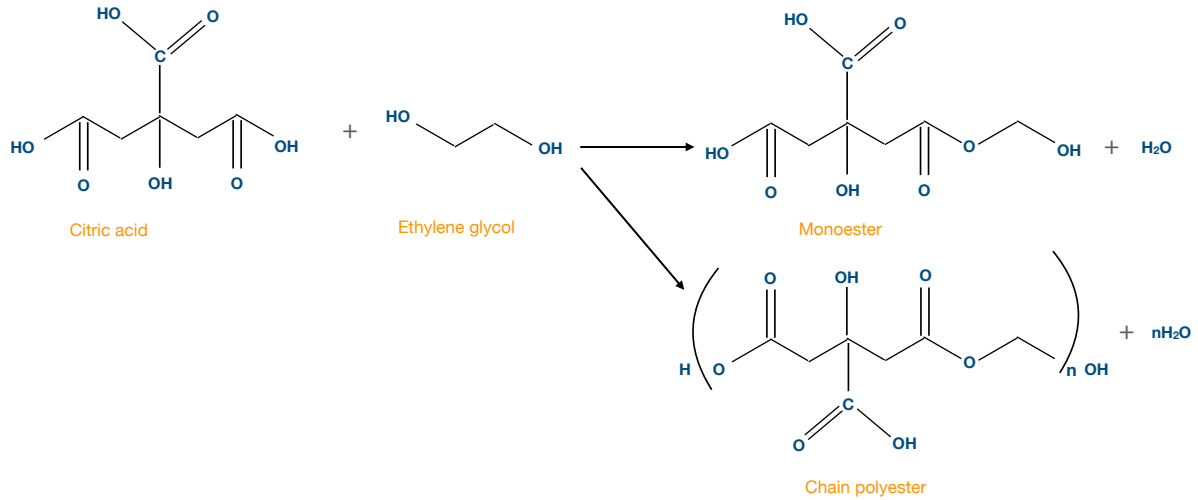


Fig. 1: Illustrating the polyesterization procedure at 85°C of the citric acid with ethylene glycol to establish chelating agent (including dehydration process) while ethylene glycol enhances the viscosity of the precursor.

2. Enterprising synthesis method, structure–morphology–superconducting–property relationship and theoretical model of ac magnetic susceptibility

2.1. Atomic-level mixing sol-gel synthesis approach

In general, the chemistry-driven sol-gel reaction represents a notable synthesis technique in producing a wide range of glassy and ceramic materials [34]. Although the ordinary procedure consists of multiple chemical transformations from a liquid solution to a gel state with a subsequent post-heat treatment, the Pechini route involves mainly distributing metallic cations with respect to chelating polymeric agents such as citric acid, lactic acid, ethylenediaminetetraacetic acid, etc. Variables within the polyesterification process are to be controlled, including (i) the chemical behavior of metallic chelation, (ii) the degrading level of free chelating compound, e.g., citric acid, (iii) the polymeric crosslinking stage, which may affect the uniformity of the cation distribution in the final gel, and (iv) the coordination structure of metal-complexes or polymer-metal-complexes in solution [34, 55]. Utilizing the polymeric precursor Pechini path, we performed in Li-doped Bi(Pb)-2223 ceramic superconductors with a nonstoichiometric formula $\text{Bi}_{1.4}\text{Pb}_{0.6}\text{Sr}_2\text{Ca}_2(\text{Cu}_{1-x}\text{Li}_x)_3\text{O}_{10+\delta}$, with $x = 0.0\text{--}0.20$ with the 0.05 increment step, and δ denotes the oxygen surplus content, in a twofold mode. For convenience, we labeled the five samples as Li0, Li5, Li10, Li15, and Li20, corresponding to the respective doping concentrations.

Stage 1: polymeric complexity Pechini trajectory. We employed the elementary recipes from aqueous solutions of high-purity nitrate salts including multivalent Bi^{3+} , Pb^{2+} , Sr^{2+} , Ca^{2+} , and Cu^{2+} , as well as monovalent doping Li^+ cations, whose molar components are equivalent to the stoichiometric formula. In preparation, precise molar amounts of nitrate salts were dissolved in the deionized aqueous solution to store separately, and the subsequent solution was mixed together to obtain a light-blue precursor. Additionally, the organic polymer precursors, so-called α -hydroxycarboxylic multicarboxyl-hydroxyl citric acid (CA), represent backbone chelating ligands for metallic cations, while polyhydroxyl ethylene glycol serves as a crosslinking agent to establish a polymeric resin in the molecular regime or chain of polymer in the esterification process, as a result, the viscosity of precursor solution constantly increases [34, 56, 57] (illustrated in Fig. 1). Upon we mixed the metallic nitrate salt solution with polymer precursor following a ratio CA : EG = 1.5 : 1, ratio CA : EG : M^{n+} = 1.5 : 1 : 1 (M^{n+} = Bi^{3+} , Pb^{2+} , Sr^{2+} , Ca^{2+} , Cu^{2+}) and stirred at 85°C on the magnetic stirrer hotplate. The water evaporated from the mixed solution at 85°C, and this favors the organic chemical reaction to the right in the formation range from monomer to polymer (Fig. 1). However, with a low temperature of 85°C, the solution prefers to form lower degree of polymeric resin [34].

The solution was intensively conglomerated and agitated at 90°C, and it was gradually added to the precursor solution to prepare stable metallic chelate complexes. Immobilization of metal complexes in such rigid organic polymer

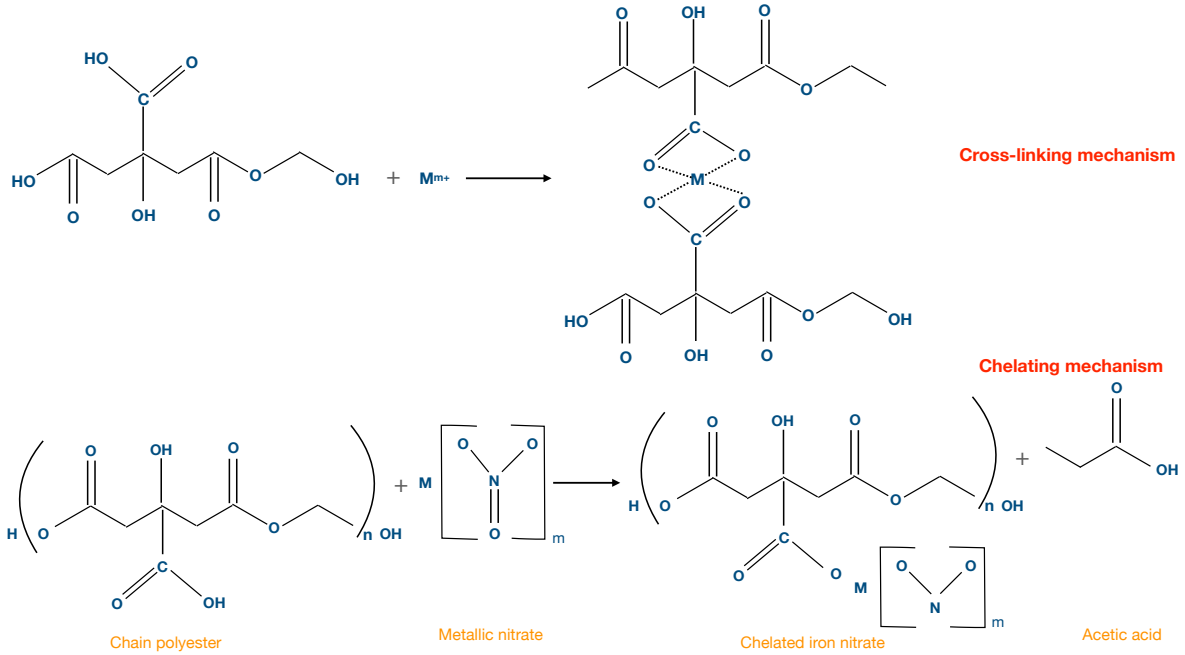


Fig. 2: Entrapping cations within polyesterisation by cross-linking and chelating mechanisms within Pechini solgel route.

networks reduces segregation of particular metal ions, ensuring compositional homogeneity [34, 56, 57]. In further heating to 120°C for 5 hours, the viscous solution was converted into a dark blue foam-like block on the bottom of the cup, accompanied by a transparent gel without any precipitation as well as completely eliminate water and organic impurities. Metallic ions therefore play a role as cross-linking agents between polymers or as a part of a chelating nitrate complex polymer as illustrated in Fig. 2. The effect of adding a monovalent Li^+ cation to the system will be tested to determine which favorable mechanism drives the Pechini formation of cross-linking or chelating pathways. Since Li^+ cations are involved, cross-linking will be more preferred under our fabrication conditions.

Stage 2: Gel pyrolysis and high- T_c phase growth. The solid precursors were pyrolyzed at 650°C for 10 hours to establish ultrafine powder precursors of the compound, in which water and other organic chelating solvents are entirely burned out in this step. After this stage, the calcined powders were ground and pressed into pellet bars under hydrostatic pressure of five tons/cm². The subsequent samples were placed inside a quartz tube furnace and sintered under atmospheric conditions at a temperature of 850°C for seven days. Compared to the standard solid-state reaction method, this stage is quite analogous in fabricating the standard high- T_c BSCCO superconductors [15, 16, 58].

2.2. Sample Characterization

In order to manifest the formation of the high- T_c Bi-2223 phase prepared by the Pechini sol-gel synthesis, we performed X-ray diffraction (XRD) spectroscopy with $\text{CuK}\alpha$ radiation to observe the crystallization of the samples as well as high- T_c phase formation and the effect of the Li doping content on the powder form. Furthermore, we characterize the surface morphology, grain size, and an insightful crystalline growth to capture for the samples utilizing Jeol-5410-LV Scanning Electron Microscope (SEM) over different scales.

Continuing, we carved specimens into square-bar shapes with the approximate dimensions of $2 \times 2 \times 12\text{mm}^3$ mimicking a wire. Subsequently, we carried out the measurements by attaching Li-doped Bi-2223 specimens on the cold finger of a Helium closed-cycle system (CTI Cryogenic 8200) and a lock-in amplifier in the range of 20–300 K. We conducted the temperature dependence of dc transport $\rho(T)$ and complex ac susceptibility $\chi(T)$ measurements ($\chi = \chi' + i\chi''$ with in-phase χ' and out-of-phase χ'' components) by an advanced four-probe and lock-in amplifier techniques, respectively. For supplemental details, we employed phase-sensitive detection within a dual-phase log-in amplifier, which allows us to measure ac susceptibility correctly and simultaneously both the imaginary and real parts

at each temperature. Whereas both coils are directly wrapped around the specimen which minimizes temperature and phase deviation, the primary coil was fed by a sinusoidal ac current with controlled magnitude and frequency to generate a homogeneous ac magnetic field and an induced voltage was measured on the secondary coil.

2.3. Theoretical analysis of ac susceptibility

It has been stated that complex ac susceptibility being a powerful tool for studying various superconductors and magnetic materials, where the frequency dependence of χ' and χ'' gives important information on the magnetic structure and the mechanism of magnetization processes [59]. The major frontier of high-temperature cuprate superconductors consists of anisotropic grains that are separated by grain boundaries that act as weak links of the Josephson network [60, 61]. Under a harmonic magnetic field $B_{ac} = B_0 \cos(\omega t)$ as a driving force, the response function of the complex AC susceptibility components consist of real and imaginary complementary parts:

$$\chi' = \frac{1}{\pi B_a} \int_0^{2\pi} M(\omega t) \cos(\omega t) d(\omega t), \quad (1)$$

$$\chi'' = \frac{1}{\pi B_a} \int_0^{2\pi} M(\omega t) \sin(\omega t) d(\omega t). \quad (2)$$

The response of such a granular superconductor to a weak magnetic field is determined by the diamagnetic response of the superconducting grains and the pinning Josephson vortices which form along grain boundaries, producing an intergranular field [13]. The effect of intergranular flux creep is incorporated into the critical state model and explains the observed frequency dependence of the ac susceptibility.

Flux pinning represents the unique characteristics of type II hard superconductors [62] in which the defects or grain boundary impurities entrap the magnetic flux, especially in sintered cuprate superconductors. That opens a possibility utilizing the effect of frequency to elucidate the properties of flux trapping in high- T_c superconductors. In the case of a long cylindrical sample with radial coordinate r , where the applied field is parallel to the cylinder axis, the critical state equation for the intergranular magnetic field profile

$$\frac{dH(r)}{dr} = \pm \frac{F_p}{|B(r)|}, \quad (3)$$

where F_p is the intergranular pinning force density of Josephson vortices. Using the Anderson flux creep model, the pinning force density is expressed as

$$F_p = \frac{k_B T}{V_b r_p} \arcsin \left[\frac{v_h}{v_0} e^{\frac{U(T,H)}{k_B T}} \right], \quad (4)$$

where $U(T, H)$ names the average intergranular pinning potential, r_p typifies the potential range and V_p is the flux bundle volume (Josephson vortices along grain boundaries), which is assumed to contain a single flux quantum Φ_0 , v_0 the attempt frequency for hopping and v_h is the ‘‘minimal-observable’’ flux line hopping rate. The minimal observable hopping rate, v_h , for an applied steady magnetic field, is the inverse of is behaved

$$v_h \approx \frac{8\Phi_0 H_{ac} \bar{R}_g^2}{R k_B T} f. \quad (5)$$

In the case of a long cylindrical sample with radius R and an applied magnetic ac field of amplitude H_{ac} , Boltzmann constant k_B and frequency f , which the activation energy will be established.

3. Results and Discussions

Once the samples were obtained, we characterized their crystal structure and surface morphology as well as probed the superconducting properties of Li-doped Bi-2223 by dc resistivity and ac susceptibility at low field equipped by a high frequency regime.

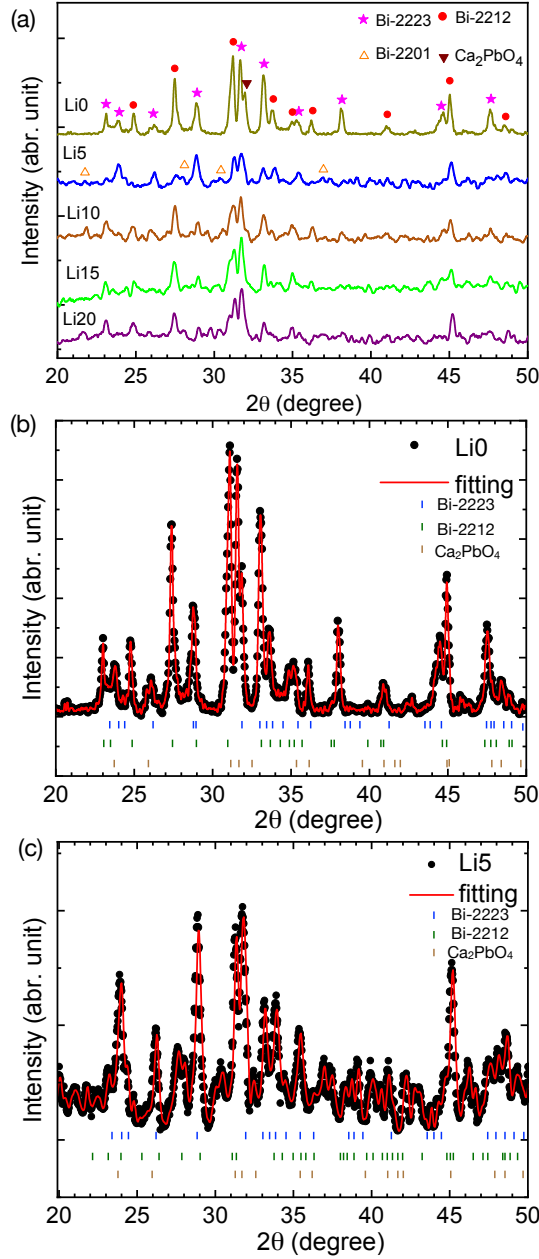


Fig. 3: (a) Series of X-ray diffraction patterns of $\text{Bi}_{1.4}\text{Pb}_{0.6}\text{Sr}_2\text{Ca}_2(\text{Cu}_{1-x}\text{Li}_x)_3\text{O}_{10+\delta}$ powders at room temperature with respect to Li-doping content up to 20 at. % replacement. Apparently, the samples consist of high- T_c triple-cuprate phase as well as amount lower- T_c double-layered Bi-2212 on surrounding boundary of grains and other impurities [63]. Rietveld refinement for (b) Li0 and (c) Li5 samples based on MAUD software.

3.1. Crystalline and surface morphology

Figs. 3(a)–(c) present a series of XRD for Li-doped Bi-2223 compounds demonstrating the major phases of Bi-2223 and 2212 together with the existing residual impurities of the liquid Ca_2PbO_4 and minor Bi-2101, together with the Rietveld refinement analysis. That is in analogy to the existence of three Bi-based superconducting phases observed in several prior sol-gel studies [14, 27, 28, 64], but different from traditional solid-state reaction or single crystal growth approaches such that only two major phases Bi-2223 and 2212 [15, 41, 43]. Nevertheless, the main diffraction peaks

Table 1: Summary of various sol-gel approaches to synthesize Pb-doped Bi-2223 superconductors and their doped counterparts, accompanied by detailed starting precursors, methods, lattice parameter, and T_c values. (The abbreviation terms are referred as CA: citric acid, EDTA: ethylenediamine tetraacetic acid, AA: acrylic acid, TF: thin film, SG: sol-gel, and SC: single crystal. Some detailed stoichiometric formulas are also noted.)

x	a Å	c Å	T_c K	H_{ac} , freq. A/m ¹ , Hz	Precursors	sintering T_s (°C), t_s (h)	Refs.
Li0 ²	3.825(6)	37.147(2)	107.4	12, 10 ⁴	nitrate, CA	air, 850, 168	Ours
Li5	3.826(3)	37.048(6)	111.4	12, 10 ⁴	nitrate, CA	air, 850, 168	Ours
Li10	3.831(1)	37.113(2)	107.6	12, 10 ⁴	nitrate, CA	air, 850, 168	Ours
Li15	3.810	37.139(0)	83.5	12, 10 ⁴	nitrate, CA	air, 850, 168	Ours
Li20	3.835(5)	37.099(5)	N/A	–	nitrate, CA	air, 850, 168	Ours
Bi-2223	3.835	37.074(4)	110.9	64, 333	nitrate, EDTA	air, 850, 100	[28]
Bi-2223+TiO ₂ (0.2%)	3.833	37.069(1)	106.4	64, 333	nitrate, EDTA	air, 850, 100	[28]
Bi-2223+TiO ₂ (0.4%)	3.832	37.064(2)	103.8	64, 333	nitrate, EDTA	air, 850, 100	[28]
Bi-2223 ³	–	–	108.2	200, 333	carbonate, EDTA	air, 835, 170	[27]
Bi-2223	–	–	107.1	200, 333	nitrate, EDTA	air, 835, 170	[27]
Bi-2223/CdO (2%)	–	–	109	5, 333	acetate	air, 845, 64	[64]
Bi2223 (2%)	–	–	108	8, 1	acetate, EDTA	air, 830/840	[26]
Bi-2223 ⁴ (TF)	–	37.1	106	–	acetate, AA	air, 860, 170	[14]
Bi-2223 (SG+SC)	3.859	37.19(1)	111	160, 0	acetate, AA	O ₂ , 500, 240	[41]

¹: With measurements using a magnetic field by Oe unit: 79.6 A/m = 1 Oe

²: Bi_{1.4}Pb_{0.6}Sr₂Ca₂Cu₃O_{10+ δ}

³: Bi_{1.64}Pb_{0.34}Sr₂Ca₂Cu₃O_{10+ δ}

⁴: Bi_{1.9}Pb_{0.35}Sr₂Ca₂Cu₃O_{10+ δ}

belong to the Bi-2223 phase (Fig. 3).

For more details, we typically observe sharp peaks ($2\theta \sim 27.5^\circ$ and 31.2°) of the double-layered Bi-2212 phase (58.5 % contribution) with only 36.7 % of Bi-2223 in the case of the undoped Li0 sample [Fig. 3(a)-(b)]. A remark is that the single sintering step at low temperature 850°C (below the eutectic point of the Bi-2223 superconductor at 870°C [65]) prepared even by an atomic mixing sol-gel route is not considered appropriate to grow pristine Bi-2223, and this has also been proven by recent fabrication of a higher sintering temperature $T_s = 860^\circ\text{C}$, providing the highest quality thin film [14]. However, with the smallest doping of Li with 5 at. % into the framework, this sintering temperature becomes suitable to grow the Bi-2223 phase (62.9 % contribution) with sharp peaks at $2\theta \sim 28.5^\circ$ and 32° . That reaffirms the reduction in the sintering temperature in Li-doped Bi-2223 samples, which complies with previous triple-layered superconductors by prior whisker fabrication and conventional solid-state synthesis [15, 53, 54]. In heavier Li-doping contents, the diffraction peak (typical $2\theta \sim 28.5^\circ$) of Bi-2223 fade rapidly, that may regard the difficulty in synthesizing monovalent Li⁺ doping by the Pechini so-gel route and as such will be elucidated in further characterizations.

As in the investigation, Bragg peaks attributed to the Li₂O crystal phase have not appeared in the XRD spectra even with high concentration of Li₂O. It may be noticed that the high content of Li₂O altered the homogeneity of the ephemeral liquid forming, the reaction rate, and as a result, the formation rate of the Bi-2223 phase. No observation of peaks related to Li-containing compounds, which means that Li₂O intercalated to the superconducting phases, either low or high, even with a large amount of impurities up to 20 at. % away from Cd-substituted for Ca in Bi-2223 compounds prepared by solgel synthesis [64].

With the spotlight on the Bi-2223 phase, based on the pseudo-tetragonal structure I4/mmm group of the Bi-2223 phase, the lattice parameters $a = 3.825\text{--}3.835$ Å and $c = 37.048\text{--}37.147$ Å are well-matched to known values ($a = 3.832\text{--}3.859$ Å and $c = 37.064\text{--}37.19$ Å [28, 41]), as we present in Table 1. This is due to the fact that the atomic radius of Li⁺ (0.73–0.76 Å) is quite equivalent to the Cu²⁺ (0.71–0.73 Å) cation. Overall, the parameters are very analogous to the existence of three Bi-based superconductive phases observed in other studies (Table 1) [14, 28].

We now consider the surface morphology with a clear grain size in large and small measuring scales (Fig. 4). At a large scale of 25 μm , we view a wide pervasive surface topography of samples accompanied by dense plates

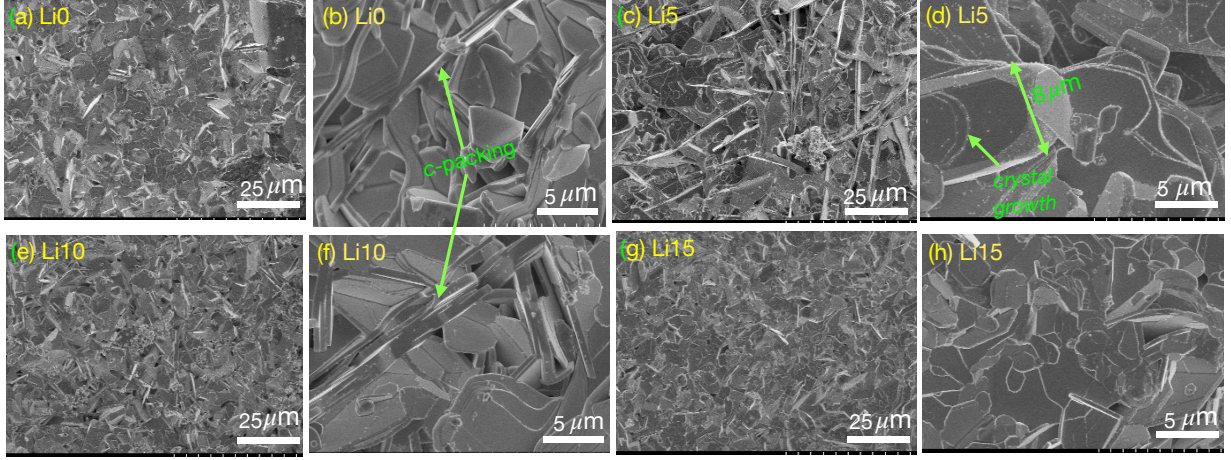


Fig. 4: Surface topography of $\text{Bi}_{1.4}\text{Pb}_{0.6}\text{Sr}_2\text{Ca}_2(\text{Cu}_{1-x}\text{Li}_x)_3\text{O}_{10+\delta}$ ceramic superconductors in terms of Li-doping content with (a)–(b) for Li0 sample, (c)–(d) for Li5, (e)–(f) for Li10 and (g)–(h) for Li15 sample.

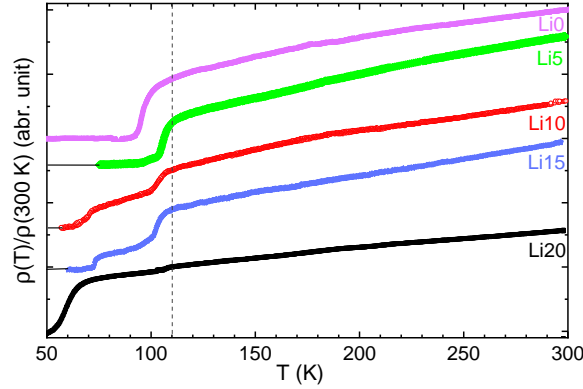


Fig. 5: Entire resistivity versus temperature $\rho(T)$ of $\text{Bi}_{1.4}\text{Pb}_{0.6}\text{Sr}_2\text{Ca}_2(\text{Cu}_{1-x}\text{Li}_x)_3\text{O}_{10+\delta}$ (with $x = 0.0\text{--}0.20$) compounds measuring in the temperature range of 50–300 K.

and needle shapes upon exposing heat and oxygen during the long-time sintering process. They behave somewhat more porous compared to the previous Li-doped in Bi-2223 prepared by a traditional solid state reaction method [15] [Figs. 4(a), (c), (e) and (g)]. However, grains prepared from sol-gel are distinct with a sharp grain boundary, while it smooths and solidifies from solid reaction counterpart at the equivalent sintering condition of 850°C [15]. A granular structure with flaky plate-like layers oriented in facet random directions is observed in the samples. In particular, Li0 and Li10 pronounce a very similar surface morphology accompanied by a random plate crystal [Figs. 4(a) and (e)], particularly showing thin c -packing granular plates with a thickness of $1\text{--}2\ \mu\text{m}$ normal to the surface [Figs. 4(b) and (f)], and that indicates the analogous superconducting properties in the next section. Notably, we capture the obvious crystalline growth on the sample surface while exposing heat and oxygen ions during the sintering process which show the preferential growth of the CuO_2 plane along the ab -plane [Fig. 4(d)]. Their surface morphology indicates the strong dark-gray color of micro-size crystal plates ($3\text{--}5\ \mu\text{m}$) and polygonal disks ($5\text{--}10\ \mu\text{m}$). Compared to the previous works, sintering at lower temperature 835°C , grain size of particles is smaller [27], or thin film under dip coating, the grain boundary is elusive [14]. Doping Cd for the Bi-2223 system even creates multiple pores on the grain as a consequence of degrading superconducting properties [64].

3.2. The effect of Li^+ substitution on superconducting properties by DC transport and ac susceptibility

DC transport measurements display normalized resistivity in the range of 50–300 K in which the shape varies following the Li-doping content in Fig. 5. Above the $T_c = 110$ K of Bi-2223, there is no observation of an abnormal point with linear resistance reduction versus temperature (see Fig. 5), providing no evidence of charge density wave phases or impurities, which belongs to strange metallic behavior, e.g., transition from metal to insulators in heavy Eu doping [66]. For samples $x = 0$ –0.15, the resistivity shows a transition of 110 K with respect to the triple-layered Bi-2223 phase, but the sharp transition is only for small doping concentrations (up to 5 at. % Li-substitution). The heavy replacement of 10–20 at. % demonstrates multiple transitions, including the amount of low- T_c single- or double-layered phases (agreeing with the above XRD study) that breaks the Bi-2223 phase formation in analogous to traditional solid-state reaction preparation [15], synthesizing Li-doped Bi-2223 by the Pechini sol-gel route faces some difficulties and challenges in establishing the high- T_c phase. The DC transport manifests that Li5 sample gives the best for resistivity shape measurement with zero resistance temperature of 100 K. That is complementary to controlling the sintering temperature from 845–860°C for thin film fabrication in which $T_s = 860$ gives the optimal result [14], while intercalating TiO_2 into Bi-2223 continuously degrades the interlinking particles as the TiO_2 content increases [28].

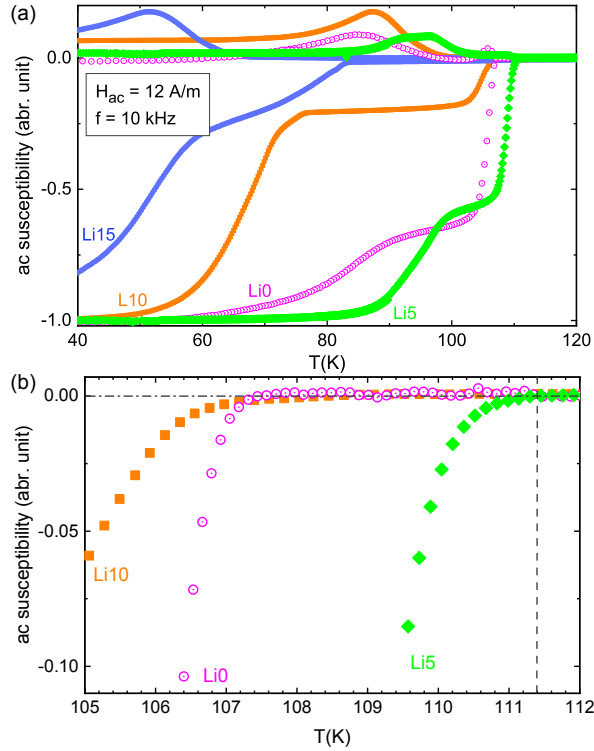


Fig. 6: (a) The magnetic susceptibility of Li-doped $\text{Bi}_{1.4}\text{Pb}_{0.6}\text{Sr}_2\text{Ca}_2\text{Cu}_3\text{O}_{10+\delta}$ ($x = 0$ –0.15) was synthesized by the Pechini sol-gel synthesis and measured at the field amplitude $H_{ac} = 12$ A/m and frequency $f = 10$ kHz. (b) Zoom in the transition region of real susceptibility around 110 K.

In addition to DC transport, we further characterize high- T_c materials by ac susceptibility which makes it a more versatile approach [67–69] to probe the detailed superconducting transition as well as the intrinsic microstructure. In Fig. 6, we perform ac susceptibility measurements for both samples through utilizing a small applied field of $H_{ac} = 12$ A/m and a frequency of 10^4 Hz for Li-doped samples in the range of 40–120 K, and each real susceptibility includes a two-step transition process of intragrain and intergrain drops. The samples $x = 0$ and $x = 0.05$ behave quite similarly to intragrain and intergrain transitions, but a higher Li-doping content deviates from them. In the circumstance of $\chi' = -1$ (Li0, Li5 and Li10 samples in Figure 6) and simultaneously, the imaginary component χ'' approaches 0, superconducting grains connect with each other via an intergrain Josephson junctions, forming a whole superconducting block in which the external magnetic field is completely shielded by the circulating persistent

supercurrent around it, known as the Meissner effect [60, 67, 69]. Therefore, this characterization is consistent with the DC transport measurement presented above.

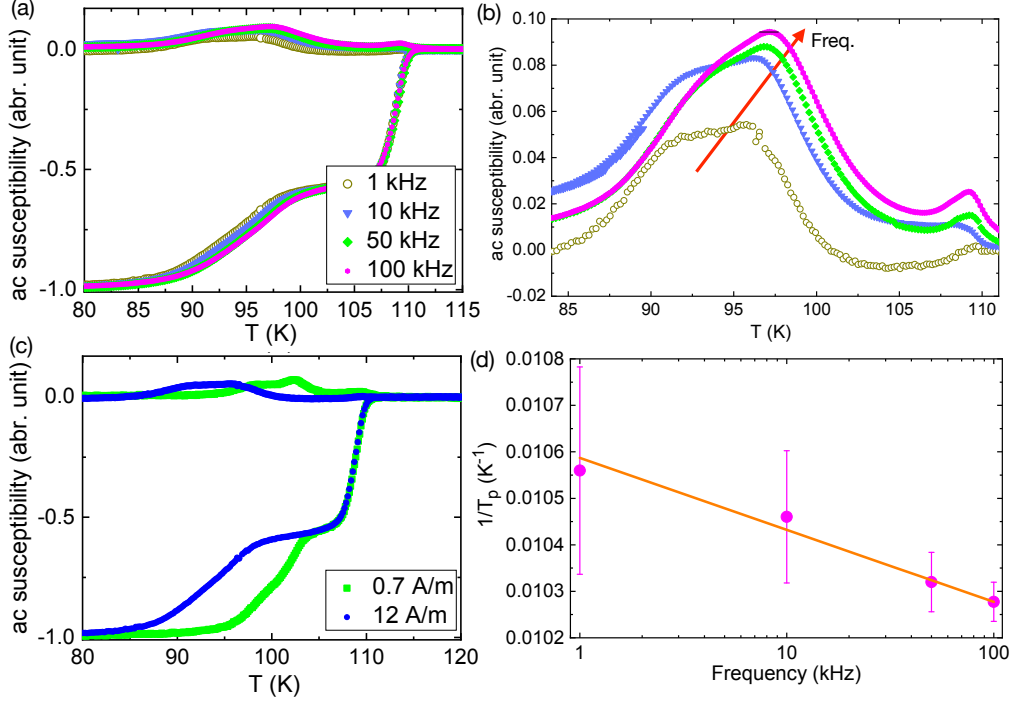


Fig. 7: The magnetic susceptibility of $\text{Bi}_{1.4}\text{Pb}_{0.6}\text{Sr}_2\text{Ca}_2\text{Cu}_{2.85}\text{Li}_{0.15}\text{O}_{10+\delta}$ (a) measured at the field amplitude $H_{ac} = 12$ A/m and frequency $f = 1$ -100 kHz, (b) zoom in detailed intergranular peak region, (c) measured at the different field amplitudes of 0.7 and 12 A/m and (d) plotting T_p versus frequency.

Upon doping Li into the Bi-2223 framework, the critical temperature advances from 107.4 K (Li0) to the peak of 111.4 K (Li5) and down to 107.6 K (Li10). Once we juxtapose the values by our Pechini route with other sol-gel approaches to elucidate the role of starting precursors and heat treatment procedure on superconducting properties. Other newly sol-gel fabrications have been applied to synthesize Bi-2223 compounds, such as starting nitrates or carbonates precursor with sintering temperature of 835°C giving $T_c = 107.1$ – 108.2 K [27], intercalating TiO_2 with sintering at 850°C producing $T_c = 103.8$ – 110.9 K [28] and sol-gel following a single crystal growth $T_c = 111$ [27] (see the list on the Table 1). We remark that the starting salt precursors have no strong effect on synthesizing high- T_c phase with starting from nitrates, carbonates or acetates, T_c is about 106–111 K. Lower sintering temperature influences the grain connectivity as well as governing lower the critical temperature. Alternation of components within the framework has a significant affect on preparation process and superconducting properties. For instance, substituting Li^+ for Cu^{2+} within Bi-2223 materials gives the critical temperature of our specimens a peak at $T_c = 111.4 \pm 0.2$ K at $x = 0.05$, while intercalating TiO_2 into the system, the critical temperature constantly reduces 110.9–103.8 K (Table 1) at quite similar starting precursors and sintering process. Thus, our specimen synthesized by the advanced Pechini method underscores slightly higher T_c by 0.5–1.5 K than preceding fabricating methods and sharp transition. With the spotlight on this impression, we pioneer the combination of appropriate doping with atomic mixing and long time sintering that play a primary role in fabricating the high quality of Bi-2223 compounds.

3.3. Low-field ac susceptibility approaching flux creep property at intergranular boundary

Considering an ac susceptibility as a function of temperature, frequency and magnetic field, we investigate the Josephson weak-link effect in Li-doped Bi-2223 superconductors by tuning frequency and ac field. In this case, we select $x = 0.05$ sample to perform and characterize the flux creep effect by implementing a wide frequency range of 1–100 kHz at a low ac magnetic field of 12 A/m [depicted in Fig. 7(a)]. Below the critical temperature, the imaginary

part of susceptibility exhibits a broad peak that is attributed to hysteresis losses at the grain boundaries and a shift of the coupling peak tends to higher temperature with increasing frequency in the 1-100 kHz range [Fig. 7(b)]. Although the intrinsic internal grain transition is pronounced intact by both the magnetic field and frequency, the intergrain transition has been heavily affected by the field amplitude [Figs. 7(a) and (c)]. The shift in the susceptibility curves was interpreted as arising from flux creep at the grain boundaries, which was first predicted by Anderson [62], following the Abrikosov theory, and heavily developed by Müller [60, 61]. In that case, the smallest possible breakdown of superconductivity caused by the motion of a quantum of magnetic flux. At appreciably higher temperatures of high- T_c Bi-2223 superconductors, thermally activated flux creep presents a significant effect [70] and the flux motion is resisted by viscous drag and inhomogeneities in the samples that pin the flux. Even with pinning magnetic quantum flux, the resistance is not exactly zero because thermally activated fluctuations can overcome pinning.

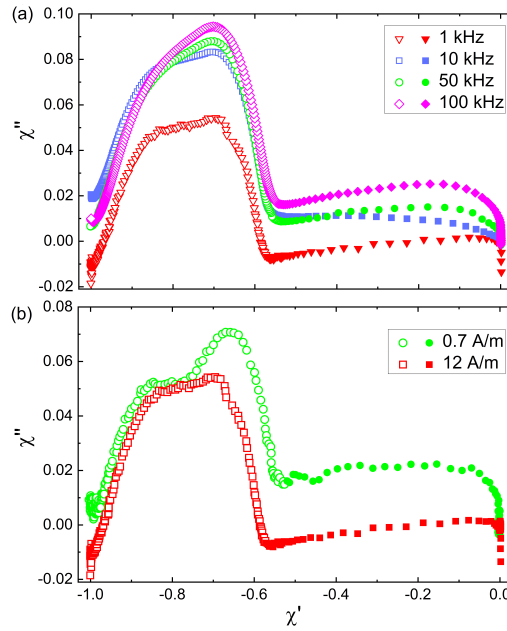


Fig. 8: The Cole-Cole plots of $\text{Bi}_{1.4}\text{Pb}_{0.6}\text{Sr}_2\text{Ca}_2\text{Cu}_{2.85}\text{Li}_{0.15}\text{O}_{10+\delta}$ was synthesized by the Pechini sol-gel synthesis and measured at (a) the field amplitude $H_{ac} = 12$ A/m and frequency $f = 1$ –100 kHz and (b) $H_{ac} = 0.7$ and 12 A/m with frequency of 10 kHz.

Anderson suggested that an energy barrier prevented the creep of flux lines [61, 62]. The activation energy ε_a is defined based on the Arrhenius equation as

$$f/f_0 = \exp(-\varepsilon_a/kT_p), \quad (6)$$

where f_0 is a constant. In the log-scale [Fig. 7(d)], the slope is calculated to be -1.55, then the activation energy is $\varepsilon_a = 0.56 \pm 0.06$ (eV) at the ac magnetic field of 12 A/m. This value is lower than the activation energy provided by 7.0–1.5 eV for the magnetic field range of 0.8–800 A/m [61]. In the samples prepared by the Pechini sol-gel synthesis, smaller energy is consumed to depin the quantum flux in terms of weak-coupling at the grain boundary which will be necessary to further improve.

Finally, the plot of the imaginary part as a function of the real branch within the harmonic susceptibility produces the Cole-Cole plot, and this kind of representation gives additional information complementary to the plot of the separate components as the ac function with respect to the temperature. In terms of the Cole-Cole representations [Figs. 8(a)–(b)], we exactly demonstrate two peaks regarding to intragrain (right lower dome) and intergrain (left higher peak) step-like transitions, the frequency on the Cole-Cole plot has much more influences than separate parts χ' and χ'' as refers to Figs. 7(a) and (c). The higher frequency makes the plot more apparent while the higher applied magnitude forms better Cole-Cole plot shape [Figs. 8(a)–(b)]. As we observed the peak height of the left dome-shaped curves grows for increasing frequencies, the phenomenon is indicated by the formation of a vortex glass phase, specified by

a collective flux creep, in contradiction to the behavior provided by simulating the Kim-Anderson flux creep model [71, 72].

4. Conclusion

In summary, we provide a concrete interpretation and synthesis pathway for growing Li-doped Bi-2223 superconductors by Pechini sol-gel methods accompanied by a single-step sintering process. Utilizing standard XRD and scanning electron microscopy, we provide insightful crystal growth as well as a slight reduction of lattice parameters for Bi-2223 compounds upon the effect of Li-doping. Due to the limitations of the Pechini chelating citric acid in producing samples containing monovalent Li^+ substitution, the critical temperature only advanced for small doping levels (0–0.5) with a value of up to 111.4 K, as determined by ac magnetic susceptibility at low fields. Compared with other sol-gel Pechini approaches, we have demonstrated a more pronounced atomic mixing synthesis to enhance the superconducting properties of high- T_c Bi-2223. The high frequency approach elucidates the activation energy of the Müller flux creep model with grain boundary and Cole-Cole plot to interpret double peaks in ac magnetic susceptibility.

References

- [1] J. Bednorz, K. Müller, Possible high- T_c superconductivity in the Ba–La–Cu–O system., *Z. Physik B - Condens. Matter* 64 (1986) 189–193. doi:10.1007/BF01303701.
- [2] J. E. Kunzler, E. Buehler, F. S. L. Hsu, J. H. Wernick, Superconductivity in Nb_3Sn at high current density in a magnetic field of 88 kGauss, *Phys. Rev. Lett.* 6 (1961) 89–91. doi:10.1103/PhysRevLett.6.89.
- [3] T. Akune, R. Maeda, N. Sakamoto, M. Takeo, Ac susceptibility in NbTi multifilamentary wires, *Phys. B: Condensed Matter* 284–288 (2000) 2095–2096. doi:10.1016/S0921-4526(99)02973-7.
- [4] G. Ryu, S. W. Kim, S. Matsuishi, H. Kawaji, H. Hosono, Superconductivity in Nb_4MSi ($m=\text{Ni, Co, and Fe}$) with a quasi-two-dimensional Nb network, *Phys. Rev. B* 84 (2011) 224518. doi:10.1103/PhysRevB.84.224518.
- [5] A.-M. Valente-Feliciano, Superconducting rf materials other than bulk niobium: a review, *Supercond. Sci. Tech.* 29 (2016) 113002. doi:10.1088/0953-2048/29/11/113002.
- [6] M. K. Wu, J. R. Ashburn, C. J. Torng, P. H. Hor, R. L. Meng, L. Gao, Z. J. Huang, Y. Q. Wang, C. W. Chu, Superconductivity at 93 K in a new mixed-phase Y-Ba-Cu-O compound system at ambient pressure, *Phys. Rev. Lett.* 58 (1987) 908–910. doi:10.1103/PhysRevLett.58.908.
- [7] J.-P. Zhou, R.-K. Lo, S. M. Savoy, M. Arendt, J. Armstrong, D.-Y. Yang, J. Talvacchio, J. T. McDevitt, Environmental degradation properties of $\text{YBa}_2\text{Cu}_3\text{O}_{7-\delta}$ and $\text{Y}_{0.6}\text{Ca}_{0.4}\text{Ba}_{1.6}\text{La}_{0.4}\text{Cu}_3\text{O}_{7-\delta}$ thin film structures, *Phys. C: Supercond.* 273 (1997) 223–232. doi:10.1016/S0921-4534(96)00631-4.
- [8] J. Roa, E. Jiménez-Piqué, J. Díaz, M. Morales, A. Calleja, M. Segarra, Corrosion induced degradation of textured YBCO under operation in high humidity conditions, *Surf. Coat. Technol.* 206 (2012) 4256–4261. doi:10.1016/j.surfcoat.2012.04.035.
- [9] H. Maeda, Y. Tanaka, M. Fukutomi, T. Asano, A new high- T_c oxide superconductor without a rare earth element, *Jpn. J. Appl. Phys.* 27 (1988) L209. doi:10.1143/JJAP.27.L209.
- [10] J. M. Tarascon, Y. LePage, L. H. Greene, B. G. Bagley, P. Barboux, D. M. Hwang, G. W. Hull, W. R. McKinnon, M. Giroud, Origin of the 110-K superconducting transition in the Bi-Sr-Ca-Cu-O system, *Phys. Rev. B* 38 (1988) 2504–2508. doi:10.1103/PhysRevB.38.2504.
- [11] Z. Wang, C. Zou, C. Lin, X. Luo, H. Yan, C. Yin, Y. Xu, X. Zhou, Y. Wang, J. Zhu, Correlating the charge-transfer gap to the maximum transition temperature in $\text{Bi}_2\text{Sr}_2\text{Ca}_{n-1}\text{Cu}_n\text{O}_{2n+4+\delta}$, *Science* 381 (2023) 227–231. doi:10.1126/science.add3672.

- [12] R. Wesche, *Physical Properties of High-Temperature Superconductors*, Wiley, 2015. doi:10.1002/9781118696644.
- [13] H. Hilgenkamp, J. Mannhart, Grain boundaries in high- T_c superconductors, *Rev. Mod. Phys.* 74 (2002) 485–549. doi:10.1103/RevModPhys.74.485.
- [14] M. Shen, L. Lei, J. Ju, H. Zong, G. Zhao, P. Ren, Preparation of high purity phase (Bi, Pb)-2223 superconducting films by sol–gel method, *Supercond. Sci. Technol.* 37 (2024) 095008. doi:10.1088/1361-6668/ad68ab.
- [15] N. K. Man, H. T. Do, Signature of T_c above 111 K in Li-doped triple-layered cuprates $\text{Bi}_{1.6}\text{Pb}_{0.4}\text{Sr}_2\text{Ca}_2(\text{Cu}_x\text{Li}_{1-x})_3\text{O}_{10+\delta}$, *Phys. Rev. Mater.* 8 (2024) 124802. doi:10.1103/PhysRevMaterials.8.124802.
- [16] A. C. Mark, D. Phelan, N. K. Man, H. T. Do, R. J. Hemley, AC electrical transport detection of magnetic properties of small, granular, and heterogeneous samples, *Rev. Sci. Instrum.* 96 (2025) 034703. doi:10.1063/5.0250005.
- [17] H. Cao, S. Zhang, Y. Cui, L. Zhi, Y. Zhang, W. Zhang, X. Liu, J. Liu, C. Li, P. Zhang, Development of a novel fabrication technique for high-quality Bi-2223 bulks with high superconducting performance, *Ceram. Int.* 50 (2024) 12212–12221. doi:10.1016/j.ceramint.2024.01.125.
- [18] S. N. Abdullah, M. M. A. Kechik, A. N. Kamarudin, Z. A. Talib, H. Baqiah, C. S. Kien, L. K. Pah, M. K. A. Karim, M. K. Shabdin, A. H. Shaari, *et al.*, Microstructure and superconducting properties of Bi-2223 synthesized via co-precipitation method: Effects of graphene nanoparticle addition, *Nanomaterials* 13 (2023) 2197. doi:10.3390/nano13152197.
- [19] S. Zhang, X. Ma, B. Shao, L. Cui, G. Liu, H. Zheng, X. Liu, J. Feng, C. Li, P. Zhang, Fabrication of multifilamentary powder in tube superconducting tapes of Bi-2223 with Sr deficient starting composition, *Cryogenics* 114 (2021) 103245. doi:10.1016/j.cryogenics.2020.103245.
- [20] H. Tsudo, Y. Miura, K. Tsuchida, A. Kato, Superconductivity of Bi Pb Sr Ca Cu O Ag systems, *Ceram. Int.* 17 (1991) 5–10. doi:10.1016/0272-8842(91)90003-I.
- [21] H. Cao, S. Zhang, Y. Cui, Y. Wang, L. Zhi, B. Shao, X. Liu, J. Liu, C. Li, J. Li, P. Zhang, Flux pinning mechanism of Bi-2223 bulk superconductors by tuning Bi-2212 and Bi-2234 intergrowths, *Ceram. Int.* 51 (8) (2025) 10014–10025. doi:10.1016/j.ceramint.2024.12.433.
- [22] S. Kobayashi, T. Kaneko, N. Ayai, K. Hayashi, H. Takei, R. Hata, Development of Bi-2223 superconducting wires, *Phys. C: Supercond. Appl.* 357-360 (2001) 1115–1118. doi:10.1016/S0921-4534(01)00523-8.
- [23] H. Ogiwara, Y. Yamada, M. Satou, T. Kitamura, T. Hasegawa, Critical current density and best transport current of an Ag-sheathed Bi-2223 tape conductor, *Ceram. Int.* 23 (1997) 1–5. doi:10.1016/0272-8842(95)00090-9.
- [24] A. Piriou, Y. Fasano, E. Giannini, O. Fischer, Effect of oxygen-doping on $\text{Bi}_2\text{Sr}_2\text{Ca}_2\text{Cu}_3\text{O}_{10+\delta}$ vortex matter: Crossover from electromagnetic to Josephson interlayer coupling, *Phys. Rev. B* 77 (2008) 184508. doi:10.1103/PhysRevB.77.184508.
- [25] N. Clayton, N. Musolino, E. Giannini, V. Garnier, R. Flükiger, Growth and superconducting properties of $\text{Bi}_2\text{Sr}_2\text{Ca}_2\text{Cu}_3\text{O}_{10}$ single crystals, *Supercond. Sci. Technol.* 17 (2004) S563. doi:10.1088/0953-2048/17/9/020.
- [26] K. Rubešová, V. Jakeš, T. Hlásek, P. Vašek, P. Matějka, Gel stabilization in chelate sol–gel preparation of Bi-2223 superconductors, *J. Phys. Chem. Solids* 73 (2012) 448–453. doi:10.1016/j.jpcs.2011.11.022.
- [27] M. Shamsodini, H. Salamati, H. Shakeripour, I. Abdolhoseini Sarsari, M. Fakhari Esferizi, H. Nikmanesh, Effect of using two different starting materials (nitrates and carbonates) and a calcination processes on the grain boundary properties of a BSCCO superconductor, *Supercond. Sci. Technol.* 32 (2019) 075001. doi:10.1088/1361-6668/ab096c.

- [28] H. Fallah-Arani, A. Sedghi, S. Baghshahi, F. shahbaz Tehrani, R. S. Moakhar, N. Riahi-Noori, N. J. Nodoushan, Bi-2223 superconductor ceramics added with cubic-shaped TiO₂ nanoparticles: Structural, microstructural, magnetic, and vortex pinning studies, *J. Alloys Compd.* 900 (2022) 163201. doi:10.1016/j.jallcom.2021.163201.
- [29] A. B. Yu, Z. Huang, W. Peng, H. Li, C. T. Lin, X. F. Zhang, L. X. You, Fabrication and transport properties of two dimensional Bi₂Sr₂Ca₂Cu₃O_{10+δ} micro-bridge, *Appl. Phys. Lett.* 120 (2022) 072601. doi:10.1063/5.0075947.
- [30] J. Chang, S. Zhang, W. Zhang, J. Liu, Q. Wang, F. Yang, C. Li, J. Li, P. Zhang, Research on the application and flux pinning of practical high-temperature superconductors, *Mater. Today Electron.* 14 (2025) 100182. doi:10.1016/j.mtelec.2025.100182.
- [31] R. Wieland, O. Kizilaslan, N. Kinev, E. Dorsch, S. Guénon, Z. Song, Z. Wei, H. Wang, P. Wu, D. Koelle, V. P. Koshelets, R. Kleiner, Terahertz emission from mutually synchronized standalone Bi₂Sr₂CaCu₂O_{8+x} infinite-Josephson-junction stacks, *Phys. Rev. Appl.* 22 (2024) 044022. doi:10.1103/PhysRevApplied.22.044022.
- [32] M. Tsujimoto, Y. Wen, Y. Maeda, A. Elarabi, Y. Simsek, U. Welp, W.-K. Kwok, S. Adachi, T. Watanabe, I. Kakeya, Terahertz emission from infinite Josephson junctions in trilayer cuprate superconductor Bi₂Sr₂Ca₂Cu₃O_{10+δ}, *Appl. Phys. Express* 18 (2025) 073001. doi:10.35848/1882-0786/adda8e.
- [33] H. Zhang, R. Wieland, W. Chen, O. Kizilaslan, S. Ishida, C. Han, W. Tian, Z. Xu, Z. Qi, T. Qing, et al., Resonant cavity modes in Bi₂Sr₂CaCu₂O_{8+x} intrinsic Josephson junction stacks, *Phys. Rev. Appl.* 11 (2019) 044004. doi:10.1103/PhysRevApplied.11.044004.
- [34] M. Kakihana, Invited review “sol-gel” preparation of high temperature superconducting oxides, *J. Sol-Gel Sci. Technol.* 6 (1996) 7–55. doi:10.1007/BF00402588.
- [35] K. Tanaka, A. Nozue, K. Kamiya, Preparation of Bi-Pb-Sr-Ca-Cu-O superconductor by the sol-gel method, *J Mater. Sci.* 25 (1990) 3551–3556. doi:10.1007/BF00575387.
- [36] B. Liang, C. Bernhard, T. Wolf, C. T. Lin, Phase evolution, structural and superconducting properties of Pb-free Bi₂Sr₂Ca₂Cu₃O_{10+δ} single crystals, *Supercond. Sci. Technol.* 17 (2004) 731. doi:10.1088/0953-2048/17/6/001.
- [37] H. Fallah-Arani, S. Baghshahi, A. Sedghi, N. Riahi-Noori, Enhancement in the performance of BSCCO (Bi-2223) superconductor with functionalized TiO₂ nanorod additive, *Ceram. Inter.* 45 (2019) 21878–21886. doi:10.1016/j.ceramint.2019.07.198.
- [38] Y. S. Lee, R. J. Birgeneau, M. A. Kastner, Y. Endoh, S. Wakimoto, K. Yamada, R. W. Erwin, S.-H. Lee, G. Shirane, Neutron-scattering study of spin-density wave order in the superconducting state of excess-oxygen-doped La₂CuO_{4+y}, *Phys. Rev. B* 60 (1999) 3643–3654. doi:10.1103/PhysRevB.60.3643.
- [39] M. G. Smith, A. Manthiram, J. Zhou, J. B. Goodenough, J. T. Markert, Electron-doped superconductivity at 40 K in the infinite-layer compound Sr_{1-y}Nd_yCuO₂, *Nature (London)* 351 (1991) 549–551. doi:10.1038/351549a0.
- [40] M. Karppinen, S. Lee, J. M. Lee, J. Poulsen, T. Nomura, S. Tajima, J. M. Chen, R. S. Liu, H. Yamauchi, Hole doping in Pb-free and Pb-substituted (Bi, Pb)₂Sr₂Ca₂Cu₃O_{10+δ} superconductors, *Phys. Rev. B* 68 (2003) 054502. doi:10.1103/PhysRevB.68.054502.
- [41] E. Giannini, V. Garnier, R. Gladyshevskii, R. Flükiger, Growth and characterization of Bi₂Sr₂Ca₂Cu₃O₁₀ and (Bi, Pb)₂Sr₂Ca₂Cu₃O_{10-δ} single crystals, *Supercond. Sci. Technol.* 17 (2003) 220. doi:10.1088/0953-2048/17/1/037.
- [42] A. Jeremie, K. Alami-Yadri, J.-C. Grivel, R. Flukiger, Bi,Pb(2212) and Bi(2223) formation in the Bi-Pb-Sr-Ca-Cu-O system, *Supercond. Sci. Technol.* 6 (1993) 73–735. doi:10.1088/0953-2048/6/10/005.

- [43] N. K. Man, N. D. Hoa, D. T. T. Nhan, Improvement of critical current density in Bi-2223 superconductor by Ag-doping, *VNU J. Sci.: Math. - Phys.* 35 (2019) 41–51. doi:10.25073/2588-1124/vnumap.4357.
- [44] K.-H. Müller, C. Andrikidis, H. K. Liu, S. X. Dou, Intergranular and intragranular critical currents in silver-sheathed Pb-Bi-Sr-Ca-Cu-O tapes, *Phys. Rev. B* 50 (1994) 10218–10224. doi:10.1103/PhysRevB.50.10218.
- [45] K.-H. Müller, C. Andrikidis, J. Du, K. E. Leslie, C. P. Foley, Connectivity and limitation of critical current in Bi-Pb-Sr-Ca-Cu/Ag tapes, *Phys. Rev. B* 60 (1999) 659–666. doi:10.1103/PhysRevB.60.659.
- [46] A. Pop, G. Ilonca, D. Ciurchea, M. Ye, I. Geru, V. Kantser, V. Pop, M. Todica, R. Deltour, Effect of Fe substitution on the magnetic and electrical properties of the $\text{Bi}_{1.6}\text{Pb}_{0.4}\text{Sr}_{1.8}\text{Ba}_{0.2}\text{Ca}_2\text{Cu}_{1-x}\text{Fe}_x\text{O}_{10}$ superconductor, *J. Alloys Compd.* 241 (1996) 116–120. doi:10.1016/0925-8388(96)02321-3.
- [47] A. V. Pop, Effect of 3d element substitution for Cu on the ac and dc magnetic properties of bulk (Bi,Pb):2223 superconductor, *Supercond. Sci. Technol.* 12 (1999) 672. doi:10.1088/0953-2048/12/10/304.
- [48] G. Ilonca, A. Pop, T.-R. Yang, T. Jurcut, C. Lung, G. Stiufluc, R. Stiufluc, I. Panfilescu, Transport properties and ac susceptibility of $\text{Bi}_{1.7}\text{Pb}_{0.4}\text{Sr}_2\text{Ca}_2(\text{Cu}_{1-x}\text{Co}_x)_3\text{O}_y$ superconductors, *Int. J. Inorg. Mater.* 3 (2001) 763–767. doi:10.1016/S1466-6049(01)00049-6.
- [49] M. Dogruer, Influence of Fe/Ca substitute on fundamental properties of $\text{Bi}_{1.8}\text{Pb}_{0.35}\text{Sr}_{1.9}\text{Ca}_{2.2-x}\text{Fe}_x\text{Cu}_3\text{O}_y$ materials, *J. Alloys Compd.* 900 (2022) 163445. doi:10.1016/j.jallcom.2021.163445.
- [50] A. Aftabi, M. Mozaffari, Thermally activated flux flow and inter-granular coupling properties in superconducting $(\text{Bi}_{1.6}\text{Pb}_{0.4}\text{Sr}_2\text{Ca}_2\text{Cu}_3\text{O}_{10+\delta})_{1-x}(\text{ZnO NPs})_x$ composites, *J. Alloys Compd.* 907 (2022) 164455. doi:10.1016/j.jallcom.2022.164455.
- [51] N. E. Suhaimi, A. Hashim, W. A. W. Razali, N. Ibrahim, S. F. Saipuddin, Superconducting and microstructure properties of Eu_2O_3 nanoparticles substitution in low density Bi(Pb)-2223 superconductor, *J. Alloys Compd.* 1012 (2025) 178448. doi:10.1016/j.jallcom.2025.178448.
- [52] A. Harabor, P. Rotaru, N. A. Harabor, Effect of ni substitute in off-stoichiometric Bi(Pb)-Sr-Ca-Cu(Ni)-O superconductor: Excess conductivity, XRD analysis and thermal behaviour, *Ceram. Int.* 45 (2019) 2742–2750. doi:10.1016/j.ceramint.2018.09.060.
- [53] I. Matsubara, T. Ogura, M. Kinoshita, Y. Hashimoto, T. Kawai, Effects of Li doping on the superconducting properties of Bi-based superconducting whiskers, *Phys. C: Supercond. Appl.* 201 (1992) 83–94. doi:10.1016/0921-4534(92)90108-0.
- [54] I. Matsubara, T. Ogura, H. Yamashita, M. Kinoshita, Li-doped Bi three-layered superconducting whiskers, *Appl. Phys. Lett.* 60 (1992) 901. doi:10.1063/1.106499.
- [55] M. Rajendran, M. Rao, Formation of BaTiO_3 from citrate precursor, *J. Solid State Chem.* 113 (1994) 239–247. doi:10.1006/jssc.1994.1366.
- [56] J. Lin, M. Yu, C. Lin, X. Liu, Multiform oxide optical materials via the versatile Pechini-type sol–gel process: Synthesis and characteristics, *J. Phys. Chem. C* 111 (2007) 5835–5845. doi:10.1021/jp070062c.
- [57] M. Kakihana, T. Okubo, Low temperature powder synthesis of LaAlO_3 through in situ polymerization route utilizing citric acid and ethylene glycol, *J. Alloys Compd.* 266 (1998) 129–133. doi:10.1016/S0925-8388(97)00445-3.
- [58] N. K. Man, T. D. Hien, N. D. Thanh, N. T. Mua, C. D. Hien, Effect of particle size on some properties of high- T_c Bi-based compounds, *J. Korean Phys. Soc.* 52 (2008). doi:10.3938/jkps.52.1625.
- [59] C. V. Topping, S. J. Blundell, A.C. susceptibility as a probe of low-frequency magnetic dynamics, *J. Phys.: Condensed Matter* 31 (2018) 013001. doi:10.1088/1361-648X/aaed96.

- [60] K. H. Müller, AC susceptibility of high temperature superconductors in a critical state model, *Phys. C: Supercond. Appl.* 159 (1989) 717–726. doi:10.1016/0921-4534(89)90143-3.
- [61] K.-H. Müller, M. Nikolo, R. Driver, Flux pinning at grain boundaries in Bi-(Pb)-Sr-Ca-Cu-O ceramic superconductors, *Phys. Rev. B* 43 (1991) 7976–7979. doi:10.1103/PhysRevB.43.7976.
- [62] P. W. Anderson, Theory of flux creep in hard superconductors, *Phys. Rev. Lett.* 9 (1962) 309–311. doi:10.1103/PhysRevLett.9.309.
- [63] A. Tampieri, G. Celotti, S. Lesca, G. Bezzi, T. M. G. La Torretta, G. Magnani, Bi(Pb)–Sr–Ca–Cu–O (2223) superconductor prepared by improved sol–gel technique, *J. Eur. Ceram. Soc.* 20 (2000) 119–126. doi:10.1016/S0955-2219(99)00158-2.
- [64] S. E. M. Ghahfarokhi, F. Joola, AC magnetic susceptibility of Cd-doped $\text{Bi}_{1.64}\text{Pb}_{0.36}\text{Sr}_2\text{Ca}_{2-x}\text{Cd}_x\text{Cu}_3\text{O}_{10}$ superconductor synthesized by the sol-gel method, *Chin. J. Phys.* 54 (2016) 921–930. doi:10.1016/j.cjph.2016.09.005.
- [65] P. Majewski, Phase diagram studies in the system Bi - Pb - Sr - Ca - Cu - O - Ag, *Supercond. Sci. Technol.* 10 (7) (1997) 453. doi:10.1088/0953-2048/10/7/001.
- [66] G. Yildirim, Beginning point of metal to insulator transition for Bi-2223 superconducting matrix doped with Eu nanoparticles, *J. Alloys Compd.* 578 (2013) 526–535. doi:10.1016/j.jallcom.2013.07.016.
- [67] R. A. Hein, T. L. Francavilla, D. H. Liebenberg, *Magnetic Susceptibility of Superconductors and Other Spin Systems*, Springer, 1991. doi:10.1007/978-1-4899-2379-0.
- [68] S. Çelebi, I. Karaca, E. Aksu, A. Gencer, Frequency dependence of the intergranular AC loss peak in a high- T_c Bi-(Pb)–Sr–Ca–Cu–O bulk superconductor, *Phys. C: Supercond. Appl.* 309 (1998) 131–137. doi:10.1016/S0921-4534(98)00531-0.
- [69] F. Gömory, Characterization of high-temperature superconductors by AC susceptibility measurements, *Supercond. Sci. Technol.* 10 (1997) 523. doi:10.1088/0953-2048/10/8/001.
- [70] M. Nikolo, R. B. Goldfarb, Flux creep and activation energies at the grain boundaries of Y-Ba-Cu-O superconductors, *Phys. Rev. B* 39 (1989) 6615–6618. doi:10.1103/PhysRevB.39.6615.
- [71] M. Polichetti, M. G. Adesso, D. Zola, J. Luo, G. F. Chen, Z. Li, N. L. Wang, C. Noce, S. Pace, Granularity and vortex dynamics in $\text{LaFeAsO}_{0.92}\text{F}_{0.08}$ probed by harmonics of the ac magnetic susceptibility, *Phys. Rev. B* 78 (2008) 224523. doi:10.1103/PhysRevB.78.224523.
- [72] M. Adesso, M. Polichetti, S. Pace, Identification of the vortex glass phase by harmonics of the AC magnetic susceptibility, *J. Phys. Chem. Solids* 67 (1) (2006) 457–459. doi:10.1016/j.jpccs.2005.10.010.